

Are Wolf-Rayet stars able to pollute the interstellar medium of galaxies? Results from integral field spectroscopy

Enrique Pérez-Montero¹, Carolina Kehrig¹, Jarle Brinchmann², José M. Vílchez¹, Daniel Kunth³, & Florence Durret³

¹ Instituto de Astrofísica de Andalucía - CSIC. Apdo. 3004, 18008, Granada, Spain

² Leiden Observatory, Leiden University, PO Box 9513, 2300 RA Leiden, The Netherlands

³ Institut d'Astrophysique de Paris, UMR 7095 CNRS, Université Pierre & Marie Curie, 98 bis boulevard Arago, 75014 Paris, France

We investigate the spatial distribution of chemical abundances in a sample of low metallicity Wolf-Rayet (WR) galaxies selected from the SDSS. We used the integral field spectroscopy technique in the optical spectral range (3700 Å–6850 Å) with PMAS attached to the CAHA 3.5 m telescope. Our statistical analysis of the spatial distributions of O/H and N/O, as derived using the direct method or strong-line parameters consistent with it, indicates that metallicity is homogeneous in five out of the six analysed objects in scales of the order of several kpc. Only in the object WR404, a gradient of metallicity is found in the direction of the low surface brightness tail. In contrast, we found an overabundance of N/O in spatial scales of the order of hundreds of pc associated with or close to the positions of the WR stars in 4 out of the 6 galaxies. We exclude possible hydrodynamical causes, such as the metal-poor gas inflow, for this local pollution by means of the analysis of the mass-metallicity relation (MZR) and mass-nitrogen-to-oxygen relation (MNOR) for the WR galaxies catalogued in the SDSS.

1. Introduction

Wolf-Rayet (WR) galaxies host very bright episodes of star formation characterized by the emission of broad WR bumps in their optical spectrum (Osterbrock & Cohen, 1982). The two main bumps in the optical range are the blue bump, centered at a wavelength of 4650 Å, produced by the emission from N^v, N^{III}, C^{III}/C^{IV} and He^{II} and associated with WC and WN stars, and the red bump which is fainter and is centered at ~ 5800 Å, produced mainly by C^{III} and C^{IV}, and associated with WC stars. The lines making up these bumps originate in the dense stellar winds from WR stars ejecting metals into the interstellar medium (ISM).

The number of known WR galaxies has tremendously increased from the discovery of the first one (He2-10: Allen et al. 1976), with different published catalogs (Conti, 1991; Schaerer et al. 1999; Guseva et al. 2000; Zhang et al. 2007) until the list of WR galaxies in the Sloan Digital Sky Survey (SDSS) by Brinchmann et al. (2008) with around 570 objects with the identification of the WR bumps in their integrated spectra.

There is an increasing evidence that the most challenging problems for this kind of objects appears in the low metallicity galaxies. Although it is well documented that the number of WR stars and the intensity of the WR bumps are higher for higher metallicities (Crowther, 2007), the values found in some low metallicity H^{II} galaxies, such as IZw18 (Legrand et al. 1997) are claimed to be much higher than those predicted by synthesis population models (*e.g.* González-Delgado et al. 2005).

Among the other important open issues regarding WR galaxies is the chemical enrichment of the ISM surrounding the stellar clusters where the WR stars are located. It is well known that there is an overabundance of the N/O ratio found in some WR nebulae (*e.g.*

Vílchez & Esteban 1991, Esteban & Vílchez 1992, Fernández-Martín et al. 2012) and also in the ISM of some WR galaxies, where the WR features are diluted (*e.g.* HS0837+4717, Pustilnik et al. 2004, NGC5253, López-Sánchez et al. 2007, other H II galaxies in Hägele et al. 2006, 2008, *green pea* galaxies, Amorín et al. 2012). Brinchmann et al. (2008) also showed that the median N/O ratio in WR galaxies with $EW(H\beta) < 100 \text{ \AA}$, has an excess of $\sim 25\%$ in relation to the other star-forming galaxies in the SDSS. Chemical evolution models do not predict high N/O values in these low-metallicity galaxies (Mollá et al. 2006), as for $12+\log(O/H) < 8.2$ most of the N in the ISM has a primary origin and therefore its chemical abundance does not depend on the metallicity of the gas, and the expected N/O ratio for closed-box models has a constant value around $\log(N/O) \approx -1.5$. However, many of these integrated observations do not allow us to properly relate the excess in some chemical species with their WR content.

To investigate the issue, among others, of the possible connection between the presence of WR stars and the chemical pollution of the surrounding ISM we have carried out a program to study metal-poor WR galaxies by means of integral field spectroscopy (IFS; Kehrig et al. 2008, Pérez-Montero et al. 2011, Kehrig et al. 2013). Integrated observations, such as long-slit or fibers, may fail to correlate the spatial location and distribution of WR features with respect to the physical conditions and the chemical abundances of the ISM as derived from the optical emission-lines. Thus, a two-dimensional analysis of the ionized material in galaxies helps us to better understand the interplay between the massive stellar population and the ISM. For instance, whether WR stars are a significant contributor to abundance fluctuations on timescales of $t \sim 10^7$ yr and to the formation of high-ionization lines (*e.g.* HeII 4686 Å) are still unsolved issues (*e.g.* Kehrig et al. 2011, Shirazi & Brinchmann, 2012) that can be probed more precisely when applying IFS to nearby galaxies (see Kehrig et al. 2013).

Thus far, the results coming from WR galaxies studied with IFS point to different scenarios, depending on the relative position between the local or extended N and/or He enrichment and the location(s) of the WR stars. López-Sánchez et al. (2011) claimed to find a local N overabundance associated with WR emission in IC-10. A similar result is found by James et al. (2013b) for the blue compact dwarf galaxy Haro 11. Monreal-Ibero et al. (2012) also find in NGC5253 local peaks of high N/O (see also Westmoquette et al. 2013), but only some of them are associated with WR emission, so this could be indicative of a different timescale between the formation of the WRs and the mixing of the ejected material with the surrounding ISM. A similar scenario is found by Kehrig et al. (2013) in Mrk178, where only one out of three detected WR clusters can be associated with an overabundance of N and He. Finally, in Pérez-Montero et al. (2011) the IFS study of N overabundant objects HS0837+4717 and Mrk930, also identified as WR galaxies, lead to high values of N/O in scales of more than 1 kpc, much beyond the power of the observed WR stars to pollute the ISM in these scales and thus pointing to other hydrodynamical processes affecting the chemistry of the gas in these galaxies, such as the infall of metal-poor gas (Köppen & Hensler, 2005). James et al. (2013a) also propose a similar scenario for their results of IFS observations of the merging galaxy UM448.

In this work we extend the sample of low-metallicity WR galaxies studied by means of IFS by six objects selected from the WR galaxy catalog by Brinchmann et al. (2008). The paper is organized as follows. In §2 we describe the observed WR galaxies and we report the IFS observations and data reduction. In §3 we present our results, including emission-line maps and derivation of oxygen and nitrogen chemical abundances and their distributions in the observed fields of view. We also describe the measurement of the WR bumps in the observed galaxies. In §4 we discuss our results about the chemical pollution

TABLE 1. The sample of observed Wolf-Rayet galaxies with different properties, including names, redshifts, positions, WR index, and date of observations with PMAS.

Name	redshift	R.A (2000)	δ (2000)	WR class	other designation	observing date
WR 038	0.0158	17h29m06.55s	+56d53m19.23s	2	SHOC 575	22-23 Jun 2009
WR 039	0.0472	17h35m01.24s	+57d03m08.55s	2	SHOC 579	25 Jun 2009
WR 057	0.0179	00h32m18.59s	+15d00m14.16s	3	SHOC 022	11 Oct 2009
WR 266	0.0213	15h38m22.00s	+45d48m07.02s	2		24-25 Jun 2009
WR 404	0.0220	21h34m37.80s	+11d25m10.19s	2	CGCG 427-004	24-25 Jun 2009
WR 505	0.0164	16h27m51.17s	+13d35m13.73s	2		22-23 Jun 2009

of ISM versus WR stars the surrounding ISM. Finally we summarize our results and present our conclusions in §5.

2. Data acquisition and reduction

2.1. Object selection and observations

We obtained IFS data of a sample of six objects selected from the SDSS WR galaxy catalog by Brinchmann et al. (2008) following three criteria: i) galaxies should be associated with a WR index of 2 (convincing WR features in the SDSS spectrum) or 3 (very clear features) in the catalog, ii) the main ionization source should be dominated by star formation as derived using diagnostic diagrams based on strong emission-lines (Baldwin et al. 1981), and iii) galaxies should have oxygen abundances lower than half the solar value [$12+\log(\text{O}/\text{H}) \approx 8.4$] as derived from the direct method, These criteria were completed with two other observational conditions: i) to have sizes smaller than the field of view (FoV) of PMAS in lens array mode $16'' \times 16''$ in order to cover the entire galaxy in one single pointing, and ii) all objects were visible from the CAHA observatory in the assigned dates at an airmass lower than 1.2. The six target WR galaxies are listed in Table 1. Column (1) quotes the names of the objects from the catalog of Brinchmann et al. (2008). Column (2) shows the redshift of each galaxy. Columns (3) and (4) give the object coordinates. Column (5) gives the WR index as done by Brinchmann et al. (2008), column (6) gives other names, and finally column (7) shows the observing date.

The data were acquired with the Integral Field Unit (IFU) Postdam Multi-Aperture Spectrophotometer (PMAS), developed at the Astrophysikalisches Institut Potsdam (Roth et al. 2005). PMAS is attached to the 3.5 m Telescope at the CAHA Observatory (Spain). The PMAS spectrograph is equipped with 256 fibers coupled to a 16×16 lens array. Each fiber has a spatial sampling of $1'' \times 1''$ on the sky resulting in a FoV of $16'' \times 16''$ collecting square areas known as spaxels.

We were awarded a service mode run on the nights 2009 June 22 - 25 (program F09-3.5-27). In addition, we continued our program with additional time on 2009 October 11th as part of the commissioning run for the new PMAS CCD.

During observations taken in 2009 June with the old PMAS $2\text{K} \times 2\text{K}$ CCD, we used the V600 grating in two separate spectral ranges: the blue side, covering a spectral range $\sim 3700\text{-}5200 \text{ \AA}$ (centered at 4500 \AA) and the red one (centered at 6325 \AA), providing a spectral range from ~ 5350 to 6850 \AA . For the galaxy WR057, taken with the new $4\text{K} \times 4\text{K}$ PMAS CCD but with the same resolution, we were able to cover the whole optical spectral range ($\sim 3700 - 6850 \text{ \AA}$) in one shot using the same V600 grating. The data were binned by a factor of 2 in the spectral direction, yielding a spectral resolution of \sim

1.6 Å/pixel. The data were acquired under non-photometric conditions and with a seeing varying between 1'' and 1''.5. To avoid major differential atmospheric refraction (DAR) effects, all expositions were taken at air mass < 1.2. We used one single pointing for each galaxy, covering in all cases the most intense burst of star formation and its surroundings. Observations of the spectrophotometric standard stars BD+253941 and PG1633 in the first run, and BD+284211 for the calibration of WR057 in the second one, were obtained during the observing nights for flux calibration. Bias frames, arc exposures (HgNe), and spectra of a continuum lamp were taken following the science exposures as part of the PMAS baseline calibrations.

2.2. Data reduction

For all objects observed with the PMAS 2K × 2K CCD, the first steps of the data reduction were done through the R3D package (Sánchez 2006). We used the P3d tool (Sandin 2010) to perform the basic data reduction of WR057, taken with the new PMAS 2K × 4K CCD. This CCD is read out in four quadrants which have slightly different gains (Kelz et al. 2006). At the time we observed WR057, P3d was the only software capable to handle the characteristics of the new CCD.

After trimming, combining the four quadrants for WR057 and bias subtraction, the expected locations of the spectra were traced on a continuum-lamp exposure obtained before each target exposure. We extracted the target spectra by adding the signal from the 5 pixels around the central traced pixel (that is the total object spectrum width). With exposures of HgNe arc lamps obtained immediately after the science exposures, the spectra were wavelength calibrated.

Fibers have different transmissions that may depend on the wavelength. The continuum-lamp exposures were used to determine the differences in the transmission fiber-to-fiber and to obtain a normalized fiber-flat image, including the wavelength dependence. This step was carried out by running the FIBER-FLAT.PL script from the R3D package. In order to homogenize the response of all the fibers, we divided our wavelength calibrated science images by the normalized fiber-flat (Sánchez 2006). Then, to remove cosmic rays, different exposures taken at the same pointing were combined using the IMCOMBINE routine in IRAF†. Flux calibration was performed using the IRAF tasks STANDARD, SENSFUNC and CALIBRATE. We co-added the spectra of the central fibers of the standard star to create a one-dimensional spectrum that was used to obtain the sensitivity function.

The reduced spectra were contained in a data cube for each object.

3. Results

3.1. Line measurements

The emission-line fluxes on the extracted one-dimensional spectra were measured for each spaxel using a Gaussian fitting over the local position of the continuum. This procedure was done using an automatic routine based on the IRAF task SPLOT. In the case of those lines with a lower signal-to-noise (S/N) (*e.g.* [O III] 4363 Å and [N II] 6584 Å), the results from this routine were revised by eye inspection and, if necessary, repeated using a manual measurement.

The adjacent continuum to each line can be affected by the underlying stellar population which can depress the intensity of the Balmer emission lines with stellar absorption

† IRAF is distributed by the National Optical Astronomical Observatories, which are operated by the Association of Universities for Research in Astronomy, Inc., under cooperative agreement with the National Science Foundation.

wings (*e.g.* Diaz 1988). This stellar absorption was studied for the brightest spaxels by fitting a combination of synthesis spectra of single stellar populations (SSP) libraries by Bruzual & Charlot (2003) and the code STARLIGHT‡ (Cid-Fernandes et al. 2004, Mateus et al. 2006). The fitted spectra were later subtracted from the observed ones and the emission-line intensities of the residuals were compared with the corresponding non-corrected values. For those objects of our sample with very high $H\beta$ equivalent widths (more than 200 Å for WR039 and around 100 Å for WR038, WR057, WR404, and WR505) the correction at $H\beta$ wavelength is negligible (less than 1 Å). Only in the case of WR266, with $EW(H\beta)$ of 54 Å, we found a correction around 4 Å for $EW(H\beta)$. For this object, appropriate corrections for each Balmer line were taken into account according to the SSP fitting in the brightest spaxels.

We calculated the statistical errors of the line fluxes, σ_l , using the expression $\sigma_l = \sigma_c N^{1/2} [1 + EW/N\Delta]^{1/2}$ (as in Pérez-Montero & Díaz 2003) where σ_c represents a standard deviation of the noise in a range centred close to the measured emission line, N is the number of pixels used in the measurement of the line flux, EW is the equivalent width of the line, and Δ is the wavelength dispersion in Å/pixel. This expression takes into account the error in the continuum and the photon count statistics of the emission line. The error measurements were performed on the extracted one-dimensional spectra. In order to minimize errors in the ratios between a certain emission line and $H\beta$, we always took first its ratio in relation to the closest hydrogen emission line (*i.e.* $H\alpha$ in the case of [NII]) and then we renormalized using the corresponding theoretical ratio (*i.e.* at the electron temperature derived in the integrated SDSS observations for each object) from Storey & Hummer (1995). We checked that the variation of this temperature across the FoV of the instrument does not introduce errors in the theoretical ratio larger than those associated with the flux of the emission lines.

3.2. Extinction correction and $H\alpha$ maps

For each fiber spectrum we derived its corresponding reddening coefficient, $c(H\beta)$, using a weighted fit to the values of the Balmer decrement derived from $H\alpha/H\beta$ and $H\gamma/H\beta$ as compared to the theoretical values expected for recombination case B from Storey & Hummer (1995) at the electron density and temperature obtained from the integrated SDSS DR-7 spectra and applying the extinction law given by Cardelli et al. (1989) with $R_V = 3.1$. In all cases, homogeneous low values of the reddening constant were derived in agreement with the same values derived from the analysis of the corresponding SDSS one-dimensional spectra.

The fluxes of the emission lines for each spaxel were corrected for extinction using its corresponding $c(H\beta)$ value. $H\alpha$ emission line maps (continuum subtracted and extinction corrected) are shown in Fig. 1. As can be seen the observed FoV encompasses the whole optical extent of our galaxies, which are mostly very compact, with the exception of WR404, which presents a cometary aspect, with a low brightness tail towards the NE direction, and WR 505, which presents several knots of star formation other than the brightest one at west of the FoV.

3.3. Oxygen and nitrogen chemical abundances

The chemical abundances of oxygen and nitrogen were studied in a representative sample of the observed spaxels in the six WR galaxies using different methods as explained below.

The most accurate method to derive oxygen abundances in emission-line objects, as

‡ The STARLIGHT project is supported by the Brazilian agencies CNPq, CAPES and FAPESP and by the France-Brazil CAPES/Cofecub program.

those in our sample, is the so-called direct method which depends on the relative intensity of both nebular oxygen emission lines to a hydrogen recombination emission-line, such as $H\beta$ (*i.e.* $[O\ II]/H\beta$ for O^+/H^+ and $[O\ III]/H\beta$ for O^{2+}/H^+), and the previous determination of the electron temperature, via the quotient between auroral-to-nebular emission lines, such as $[O\ III]\ 4363\ \text{\AA}$ and $[O\ III]\ 5007\ \text{\AA}$. See, for instance, Pérez-Montero et al. (2011) or Kehrig et al. (2013) for additional details of this procedure and how to calculate the low-excitation electron temperature to derive low-excitation ionic abundances. This method was applied to the SDSS DR7 spectra of the brightest regions of the six observed galaxies leading to values of the total oxygen abundances compatible with the low metallicity regime. Owing to the spectral coverage in the SDSS spectra (3800-9100 \AA), the $[O\ II]\ 3727\ \text{\AA}$ emission-line was not detected in WR038, WR057, and WR505, and the $[O\ II]\ 7319, 7330\ \text{\AA}$ were used instead, as described in Kniazev et al. (2002). The total abundances derived in the SDSS spectra using this method are listed in Table 2.

Regarding the PMAS IFS observations, the direct method was applied in a representative number of spaxels only in WR039, where the $[O\ III]\ 4363\ \text{\AA}$ emission line was detected with acceptable S/N (> 2.5). In the other galaxies of our sample, the direct method could only be applied in the brightest spaxels in WR038, WR057, and WR505 and in none of them in WR266 and WR404.

Therefore, the spatial analysis of the chemical properties in these galaxies was done by means of strong-line methods. We first resorted to the N2 parameter (*e.g.* Denicoló et al. 2002), defined as the ratio between $[N\ II]\ 6584\ \text{\AA}$ and $H\alpha$. This parameter has the advantage that it does not depend on reddening nor flux calibration uncertainties and is linearly well correlated with oxygen abundance up to solar metallicities. On the contrary it has an important drawback when it is used for extended objects, as those studied in this work by means of IFS, as it also varies as a function of the excitation conditions (Pérez-Montero & Díaz 2005). We verified in what objects this method could be applied to derive reliably the spatial distribution of the oxygen abundance, by plotting in Figure 2 the relation between the N2 parameter and the $[O\ II]/[O\ III]$ ratio, which traces the nebular excitation. As can be seen, in the most extended objects of our sample, WR404 and WR505, there is a clear correlation between these two emission-line ratios. In the other objects there is no clear relation between them, with the possible exception of WR057, but in this object the spatial variation of N2 is lower than the observational errors. Hence, in the case of WR404 and WR505 galaxies, we used the strong-line parameter O3N2, firstly introduced as a metallicity calibrator by Alloin et al. (1979) and which is defined as the emission-line ratio between $[O\ III]\ 5007\ \text{\AA}$ and $[N\ II]\ 6584\ \text{\AA}$. According to several authors, such as Pettini & Pagel (2004) or Pérez-Montero & Contini (2009), this parameter is not valid for very low metallicity objects ($12+\log(O/H) < 8.0$) but, on the contrary, its dependence on excitation is much lower than in the case of N2. According to the values derived from the SDSS spectra for WR404 and WR505, their mean oxygen abundances are higher than the lower limit for O3N2, so this parameter was used for these two objects instead.

For the sake of consistency between the three employed methods (direct method in the case of WR039, N2 parameter for WR038, WR057, and WR266, and O3N2 for WR404 and WR505) we used the calibrations presented in Pérez-Montero & Contini (2009) for N2 and O3N2, which are consistent with the direct method. The resulting oxygen abundance maps of the six observed galaxies are plotted in Figure 3 along with the histogram distributions of the abundances in those spaxels with enough S/N in all the involved emission lines ($S/N > 2.5$).

In the case of the nitrogen-to-oxygen ratio (N/O) the direct method can also be used

TABLE 2. Total oxygen abundances and N/O derived for the six studied WR galaxies using different methods as described in the text. The confidence level from the Lilliefors test for those spaxels where all involved emission-lines were measured is the p-value. Column (3) lists the mean value and standard deviation (sigma) from the Gaussian fit as long as p-value > 0.05; otherwise the mean value and sigma of the data distribution are shown. Column (4) and (5) show the O/H and N/O, and their corresponding errors derived from the brightest spaxel and from the SDSS spectrum for each galaxy, respectively. The number in parenthesis indicates the method used to derive the chemical abundances: (1) from direct method with [O II] 3727 Å, (2) from direct method with [O II] 7319,7330 Å, (3) from N2, (4) from O3N2, and (5) from N2O2 .

	p-value	mean ± st. deviation	brightest	SDSS
<hr/>				
12+log(O/H)				
WR 038	0.51	8.14 ± 0.06 (3)	8.09 ± 0.07 (1)	8.16 ± 0.11 (2)
WR 039	0.07	8.06 ± 0.09 (1)	7.96 ± 0.05 (1)	8.13 ± 0.05 (1)
WR 057	0.10	7.94 ± 0.06 (3)	8.14 ± 0.10 (1)	8.06 ± 0.06 (2)
WR 266	0.23	8.23 ± 0.05 (3)	8.26 ± 0.30 (1)	8.18 ± 0.14 (1)
WR 404	0.02	8.26 ± 0.02 (4)	8.23 ± 0.30 (4)	8.23 ± 0.05 (1)
WR 505	0.30	8.31 ± 0.06 (4)	8.16 ± 0.16 (4)	8.09 ± 0.08 (2)
<hr/>				
log(N/O)				
WR 038	0.01	-1.14 ± 0.14 (5)	-0.87 ± 0.27 (1)	-1.06 ± 0.24 (2)
WR 039	0.04	-1.09 ± 0.09 (1)	-0.80 ± 0.20 (1)	-1.17 ± 0.14 (1)
WR 057	0.39	-1.42 ± 0.07 (5)	-1.48 ± 0.26 (1)	-1.32 ± 0.15 (2)
WR 266	0.04	-1.29 ± 0.10 (5)	-1.13 ± 0.30 (1)	-1.18 ± 0.24 (1)
WR 404	0.00	-1.37 ± 0.07 (5)	-1.39 ± 0.30 (5)	-1.40 ± 0.06 (1)
WR 505	0.00	-1.21 ± 0.15 (5)	-1.15 ± 0.38 (5)	-1.27 ± 0.16 (2)

to derive the N^+/H^+ ratio and then deriving N/O using the approximation $N^+/O^+ \approx N/O$ [as before see further details in Pérez-Montero et al. (2011) or Kehrig et al. (2013)], but this method could only be used in a representative number of spaxels in WR039. For the other five galaxies we resorted to the N2O2 parameter, defined as the ratio of [N II] 6584 Å and [O II] 3727 Å. This ratio has the advantage that it has a monotonic linear relation with N/O and, contrary to N2, it does not have any dependence on excitation as it only depends on low-excitation emission-lines. As in the case of oxygen abundances, we used the empirical calibration of N2O2 with N/O from Pérez-Montero & Contini (2009), which is consistent with the direct method derivations of this chemical abundance ratio. The resulting N/O maps of the six observed galaxies are plotted in Figure 4 along with the histogram distributions of the abundances in those spaxels with enough S/N in all the involved emission lines.

3.4. Spatial chemical homogeneity

To study to what extent the chemical content of the gas can be considered as homogeneous, and to give the statistical significance of the O/H and N/O distributions, we used the procedure presented in Pérez-Montero et al. (2011) and refined in Kehrig et al. (2013). This method is based on the assumption that a certain property can be considered as spatially homogeneous across the observed FoV if two conditions are satisfied: for the corresponding dataset (i) the null hypothesis (*i.e.* the data come from a normally distributed population) of the Lilliefors test (Lilliefors, 1967) cannot be rejected at the 5% significance level, and (ii) the observed variations of the data distribution around the single mean value can be explained by random errors; *i.e.* the corresponding Gaussian sigma should be lower or of the order of the typical uncertainty of the considered prop-

erty; we take as typical uncertainty the square root of the weighted sample variance. In Table 2 we show the results from our statistical analysis for both total O/H and N/O.

The Lilliefors test for each of the distributions was performed on the linear values of the chemical abundances. The corresponding confidence levels (p-values) are listed in Table 2 with the resulting means and Gaussian sigma in case that the p-value is higher than 0.05. Otherwise, the means and standard deviations are those of the distributions. In those cases where the p-value is larger than 0.05, the second condition imposed to consider a homogeneous distribution is also satisfied in all cases. In all distributions where a strong-line method was used to derive both O/H and N/O, the sigma of the Gaussian is much lower than the intrinsic uncertainty associated with these methods (~ 0.3 dex). For WR039, where the direct method was used the weighted sigma for both oxygen abundance and N/O is 0.2 dex, which also is larger than the usual sigmas in the Gaussian fittings.

4. Discussion: are WR stars able to pollute the ISM of galaxies?

The use of IFS is fundamental to study the spatial extent of the chemical properties of the ISM in extended objects. In this context, this technique along with the use of appropriate statistical tools allows us to explore the presence of chemical inhomogeneities in both O/H and N/O, and to relate this local pollution with the position of WR stars, whose stellar winds enrich the surrounding ISM with the products of the main sequence nuclear burning of massive stars.

Our statistical method points to a high degree of homogeneity in O/H across the FoV of the studied galaxies, implying scales of several kpc, with the only exception of WR404, where a possible gradient of metallicity is found. This spatial variation of the metallicity goes from lower values in the brightest region of the galaxy at the SE, to slightly higher values in the low surface brightness tail towards the NW.

Our spatial analysis of N/O reveals that only WR057 presents values for which the homogeneity of this abundance ratio cannot be ruled out. In contrast, for all the other cases the conditions assumed to consider a homogeneous distribution of N/O are not fulfilled, as very high values of this ratio in certain positions of the FoV were measured.

Although the WR blue bump is detectable in the SDSS spectra of the six selected galaxies, we only found it in our PMAS observations in two spaxels of the WR039 galaxy. These are marked with red crosses in Figure 1. A thorough analysis of the causes of the missing detection of the bump in the other objects will be performed in a forthcoming paper. Figure 5 shows a portion of the spectrum obtained by co-adding the emission from the 2 spaxels with the WR bump detection. The measured luminosity of the bump at the adopted distance, once the emission lines over the bump were removed, [$L_{\text{WR}} = 10^{40.08 \pm 0.08}$ erg/s], is consistent with the value measured in the integrated SDSS spectrum [$L_{\text{WR}} = 10^{39.97 \pm 0.15}$ erg/s]. In contrast, the equivalent width of the bump in these two spaxels (20 ± 4 Å) is much higher than in the SDSS spectrum (8 ± 4 Å), as expected taking into account the fact that the collected stellar continuum in the area of the two 1" PMAS spaxels is fainter than in the 3" SDSS fiber.

To investigate the possible connection between the detected nitrogen overabundance and the location of the WR stars, we identified in the histograms shown in Figure 3 and 4 the probable positions of the WR stars. In the case of WR039, where the WR bump was detected in our IFS data, the corresponding spaxels with WR emission are plotted as red bars. In the rest of the objects, we selected the four spaxels probably encompassed by the SDSS fiber and which are thought to host the WR population, and we plotted them in the histograms as black bars. This subset of spaxels always include

the brightest $H\alpha$ position in the observed galaxies. Finally, to study the possible extent of the N pollution, we also identified the 12 spaxels around these 4 positions of the SDSS fiber as brown bars in the histograms. As can be seen in the histograms and can also be confirmed by visual inspection of the N/O maps, the nitrogen overabundance is tightly related to the position of the WRs in WR038, WR039, WR266, and WR505, although there is not a perfect match between them. This is well illustrated in the unique case where we identified the WR emission, WR039, where the N overabundance is slightly displaced in relation to the position of the WR bumps. The other galaxy whose N/O is not homogeneous is WR404, but in this case, this is probably related to the gradient of metallicity across its tail detected in the O/H analysis, as no direct relation between the N overabundance and the positions of the WRs is detected.

The results obtained in this work, in which we find evidence for a local nitrogen overabundance (in zones of the order of 100 pc around the position of the WR bumps) in four out of the six observed galaxies by means of IFS have the following implications:

- WR stars are possibly the main cause of the overabundance of nitrogen observed in 4 out of 6 observed galaxies at spatial scales of the order of several hundreds of parsecs detected around the position of these stars, differing from the objects studied in Pérez-Montero et al. (2011) where this overabundance was detected at scales of several kpc. According to the chemical yields of massive stars from Mollá & Terlevich (2012) presented in Figure 14 of Pérez-Montero et al. (2011) the stellar masses of the ionizing clusters in the sample of WR galaxies studied here, (all of them around $10^7 M_{\odot}$) can produce a N/O excess at distances compatible with the scales at which the N pollution has been detected by means of IFS in this work.

- As the local N pollution has not been observed in all the studied objects in this work and, in those where it was observed, it does not show a perfect match with the positions of the WR bump. Although it is necessary to take the limited spatial resolution of our observations into account, this mismatch could be possibly due to a timescale offset between the lifetime of the WR stars and the mixing of the ejected material with the ISM. Possibly, the positions with relatively high N/O trace regions where the WR stars were present. In contrast, the positions where the bumps are detected are tracing the ongoing star formation regions. This spatial mismatch between N excess and WR positions has also been observed in other nearby star-forming objects studied by means of optical IFS (*e.g.* NGC5253, Monreal-Ibero et al. 2012). This timescale offset between WR lifetimes and N mixing is supported by the results from other previous works based on IFS data where WR stars were reported, but not the excess in N/O (*e.g.* in this work, WR057 and WR404, in HS0837+4717 and Mrk930 in Pérez-Montero et al. 2011, or in two out of the three WR clusters detected in Mrk178 (Kehrig et al. 2013).

- The local nitrogen pollution happens while homogeneous values of the oxygen abundance are found, which could be indicative that oxygen is not noticeably present in the winds ejected by the WR stars at this stage. Apparently the properties of these winds (density, velocity, etc ...) favour the mixing of their components with the surrounding warm ISM. However, the mixing expected later of the oxygen ejected during the last stages of the WR phase and the subsequent O-rich SNe explosions have a timescale much longer than that of early WR winds (*e.g.* Tenorio-Tagle 1996).

- Additional mechanisms other than the enrichment due to WR winds are thought to be responsible for the nitrogen overabundance in star-forming galaxies. This is the case of collisional deexcitation of O^+ in strong shocks associated with mergers (Raymond 1979) or other hydrodynamical processes, such as the infall of pristine gas (Köppen & Hensler, 2005), which can at same time reduce the overall metallicity of galaxies and boost the star-formation. These processes could be behind the relation between metallicity and

star-formation rate in galaxies. On the contrary, such a mechanism will not have any influence on the abundance ratio of metals as N and O (Edmunds 1990). A very suitable tool to identify these processes and to distinguish them from local pollution, as in the case of N ejection by WR stars, is the simultaneous analysis of the relations between stellar mass and metallicity (MZR) and with N/O (MNOR). This was already used by Amorín et al. (2010) to understand the low metallicity combined with N/O ratio much higher than the values in the plateau of the diagram O/H vs. N/O measured in *green pea* galaxies. In that work the analysis of these galaxies shows that these objects have the expected N/O for their masses, while they have systematically lower metallicities, even though WR stars have been detected in deep GTC spectra of some of them (Amorín et al. 2012).

Hence, for WR galaxies, we try to understand their average observed N/O excess, as reported by Brinchmann et al. (2008), doing the same analysis. In Figure 6 is shown the MZR for the star-forming galaxies of the SDSS, with their stellar masses compiled from the Max Planck Institute for Astrophysics-Johns Hopkins University (MPA-JHU) catalog[†] and oxygen abundances calculated using the N2 parameter for emission lines with S/N larger than 2. The solid red line, as explained in Pérez-Montero et al. (2013) is a quadratic fit to the medians for stellar mass bins of 0.2 dex. The black points are the matches between the WR galaxy catalog by Brinchmann et al. (2008) and all the other star-forming SDSS galaxies selected from the MPA/JHU list. The number of matches obeying the S/N criterion and having a minimum redshift ($z > 0.02$) to avoid serious aperture effects in the determination of the stellar mass, as described in Pérez-Montero et al. (2013), is 254. In the right panel of the same figure is shown the MNOR, as calculated using the N2S2 parameter with the calibration by Pérez-Montero & Contini (2009). As can be appreciated, and contrary to *green pea* galaxies, the WR galaxies are in average in agreement with the metallicities expected for their stellar mass but, in contrast, have larger N/O ratios, which could be just local pollution values in the same region covered by the SDSS fiber and possibly due to the enrichment by WR stars.

5. Summary

In this work we presented 3.5 m CAHA - PMAS IFS observations of six metal-poor compact WR galaxies selected from the catalog published by Brinchmann et al. (2008) in the optical spectral range 3700 - 6850 Å. Our aim is to study the connection between the presence of WR stars and N/O excess as compared with the values predicted by chemical evolution models at this metallicity regime.

We derived O/H and N/O abundances ratios using the direct method (*i.e.* with the determination of the electron temperature), or strong-line methods based on [N II]6584 Å emission line, such as N2, O3N2 (for O/H), and N2O2 (for N/O) with the calibrations provided by Pérez-Montero & Contini (2009), which are consistent with the direct method. We studied the homogeneity of the spatial distributions of both O/H and N/O using the same statistical procedure introduced by Pérez-Montero et al. (2011) and improved by Kehrig et al. (2013).

Our results indicate that in all the studied objects O/H can be considered as uniform in scales of the order of several kpc, with the exception of WR404, for which a gradient of O/H is found in the same direction of a low surface brightness tail. In contrast, N/O can only be considered as homogeneous in WR057. In four of the six studied galaxies (WR038, WR039, WR266, and WR505) we found positions associated with or close to

[†] Available at <http://www.mpa-garching.mpg.de/SDSS/>

the WR stars with N excess in spatial scales of the order of several hundreds of pc. We discussed that, according to the models presented by Pérez-Montero et al. (2011) based on massive star yields of Mollá & Terlevich (2012), the N excess length scale is consistent with the distances at which the stellar clusters in these galaxies can enhance the gas-phase abundance of N. On the other hand, our analysis of both the MZR and the MNOR of the WR galaxies of the SDSS WR catalog of Brinchmann et al. (2008) excludes hydrodynamical effects, such as metal-poor gas inflows, as the more frequent cause of the N excess detected in the SDSS galaxies with a detection of the WR bump.

Based on observations collected at the Centro Astronómico Hispano Alemán (CAHA) at Calar Alto, operated jointly by the Max-Planck Institut für Astronomie and the Instituto de Astrofísica de Andalucía (CSIC). This work has been partially supported by projects AYA2007-67965-C03-02 and AYA2010-21887-C04-01 of the Spanish National Plan for Astronomy and Astrophysics. We also thank an anonymous referee for his/her very thorough revision of this manuscript that has helped to improve it.

REFERENCES

- Allen, D. A., Wright, A. E., & Goss, W. M. 1976, *MNRAS*, 177, 91
- Alloin, D., Collin-Souffrin, S., Joly, M., & Vigroux, L. 1979, *A&A*, 78, 200
- Amorín, R. O., Pérez-Montero, E., & Vílchez, J. M. 2010, *ApJL*, 715, L128
- Amorín, R., Pérez-Montero, E., Vílchez, J. M., & Papaderos, P. 2012, *ApJ*, 749, 185
- Baldwin, J. A., Phillips, M. M., & Terlevich, R. 1981, *PASP*, 93, 5
- Brinchmann, J., Kunth, D., & Durret, F. 2008, *A&A*, 485, 657
- Bruzual, G., & Charlot, S. 2003, *MNRAS*, 344, 1000
- Cardelli, J. A., Clayton, G. C., & Mathis, J. S. 1989, *ApJ*, 345, 245
- Cid Fernandes, R., Gu, Q., Melnick, J., et al. 2004, *MNRAS*, 355, 273
- Conti, P. S., Garmany, C. D., & Massey, P. 1989, *ApJ*, 341, 113
- Crowther, P. A. 2007, *ARA&A*, 45, 177
- Denicoló, G., Terlevich, R., & Terlevich, E. 2002, *MNRAS*, 330, 69
- Díaz, A. I. 1988, *MNRAS*, 231, 57
- Edmunds, M. G. 1990, *MNRAS*, 246, 678
- Esteban, C., & Vílchez, J. M. 1992, *ApJ*, 390, 536
- Fernández-Martín, A., Martín-Gordón, D., Vílchez, J. M., et al. 2012, *A&A*, 541, A119
- González Delgado, R. M., Cerviño, M., Martins, L. P., Leitherer, C., & Hauschildt, P. H. 2005, *MNRAS*, 357, 945
- Guseva, N. G., Izotov, Y. I., & Thuan, T. X. 2000, *ApJ*, 531, 776
- Hägele, G. F., Díaz, Á. I., Terlevich, E., et al. 2008, *MNRAS*, 383, 209
- Hägele, G. F., Pérez-Montero, E., Díaz, Á. I., Terlevich, E., & Terlevich, R. 2006, *MNRAS*, 372, 293
- James, B. L., Tsamis, Y. G., Walsh, J. R., Barlow, M. J., & Westmoquette, M. S. 2013, *MNRAS*, 430, 2097
- James, B. L., Tsamis, Y. G., Barlow, M. J., Walsh, J. R., & Westmoquette, M. S. 2013, *MNRAS*, 428, 86
- Kehrig, C., Oey, M. S., Crowther, P. A., et al. 2011, *A&A*, 526, A128
- Kehrig, C., Pérez-Montero, E., Vílchez, J. M., et al. 2013, *MNRAS*, 432, 2731
- Kehrig, C., Vílchez, J. M., Sánchez, S. F., et al. 2008, *A&A*, 477, 813
- Kelz, A., Verheijen, M. A. W., Roth, M. M., et al. 2006, *PASP*, 118, 129
- Kniazev, A. Y., Grebel, E. K., Hao, L., et al. 2003, *ApJL*, 593, L73
- Köppen, J., & Hensler, G. 2005, *A&A*, 434, 531
- Legrand, F., Kunth, D., Roy, J.-R., Mas-Hesse, J. M., & Walsh, J. R. 1997, *A&A*, 326, L17
- Lilliefors, H. W., 1967, *J. Amer. Statistical Assoc.*, 62, 399

- López-Sánchez, Á. R., Esteban, C., García-Rojas, J., Peimbert, M., & Rodríguez, M. 2007, ApJ, 656, 168
- López-Sánchez, Á. R., Mesa-Delgado, A., López-Martín, L., & Esteban, C. 2011, MNRAS, 411, 2076
- Mateus, A., Sodr e, L., Cid Fernandes, R., et al. 2006, MNRAS, 370, 721
- Moll a, M., & Terlevich, R. 2012, MNRAS, 425, 1696
- Moll a, M., V lchez, J. M., Gavil an, M., & D az, A. I. 2006, MNRAS, 372, 1069
- Monreal-Ibero, A., Walsh, J. R., & V lchez, J. M. 2012, A&A, 544, A60
- Osterbrock, D. E., & Cohen, R. D. 1982, ApJ, 261, 64
- P rez-Montero, E., & Contini, T. 2009, MNRAS, 398, 949
- P rez-Montero, E., Contini, T., Lamareille, F., et al. 2013, A&A, 549, A25
- P rez-Montero, E., & D az, A. I. 2005, MNRAS, 361, 1063
- P rez-Montero, E., & D az, A. I. 2003, MNRAS, 346, 105
- P rez-Montero, E., V lchez, J. M., Cedr es, B., et al. 2011, A&A, 532, A141
- Pettini, M., & Pagel, B. E. J. 2004, MNRAS, 348, L59
- Pustilnik, S., Kniazev, A., Pramskij, A., et al. 2004, A&A, 419, 469
- Raymond, J. C. 1979, ApJS, 39, 1
- Roth, M. M., Fechner, T., Wolter, D., et al. 2010, SPIE, 7742,
- S nchez, S. F. 2006, Astronomische Nachrichten, 327, 850
- Sandin, C., Becker, T., Roth, M. M., et al. 2010, A&A, 515, A35
- Schaerer, D., Contini, T., & Pindao, M. 1999, A&A, 136, 35
- Shirazi, M., & Brinchmann, J. 2012, MNRAS, 421, 1043
- Storey, P. J., & Hummer, D. G. 1995, MNRAS, 272, 41
- Tenorio-Tagle, G. 1996, AJ, 111, 1641
- Vilchez, J. M., & Esteban, C. 1991, Wolf-Rayet Stars and Interrelations with Other Massive Stars in Galaxies, 143, 379
- Westmoquette, M. S., James, B., Monreal-Ibero, A., & Walsh, J. R. 2013, A&A, 550, A88
- Zhang, W., Kong, X., Li, C., Zhou, H.-Y., & Cheng, F.-Z. 2007, ApJ, 655, 851

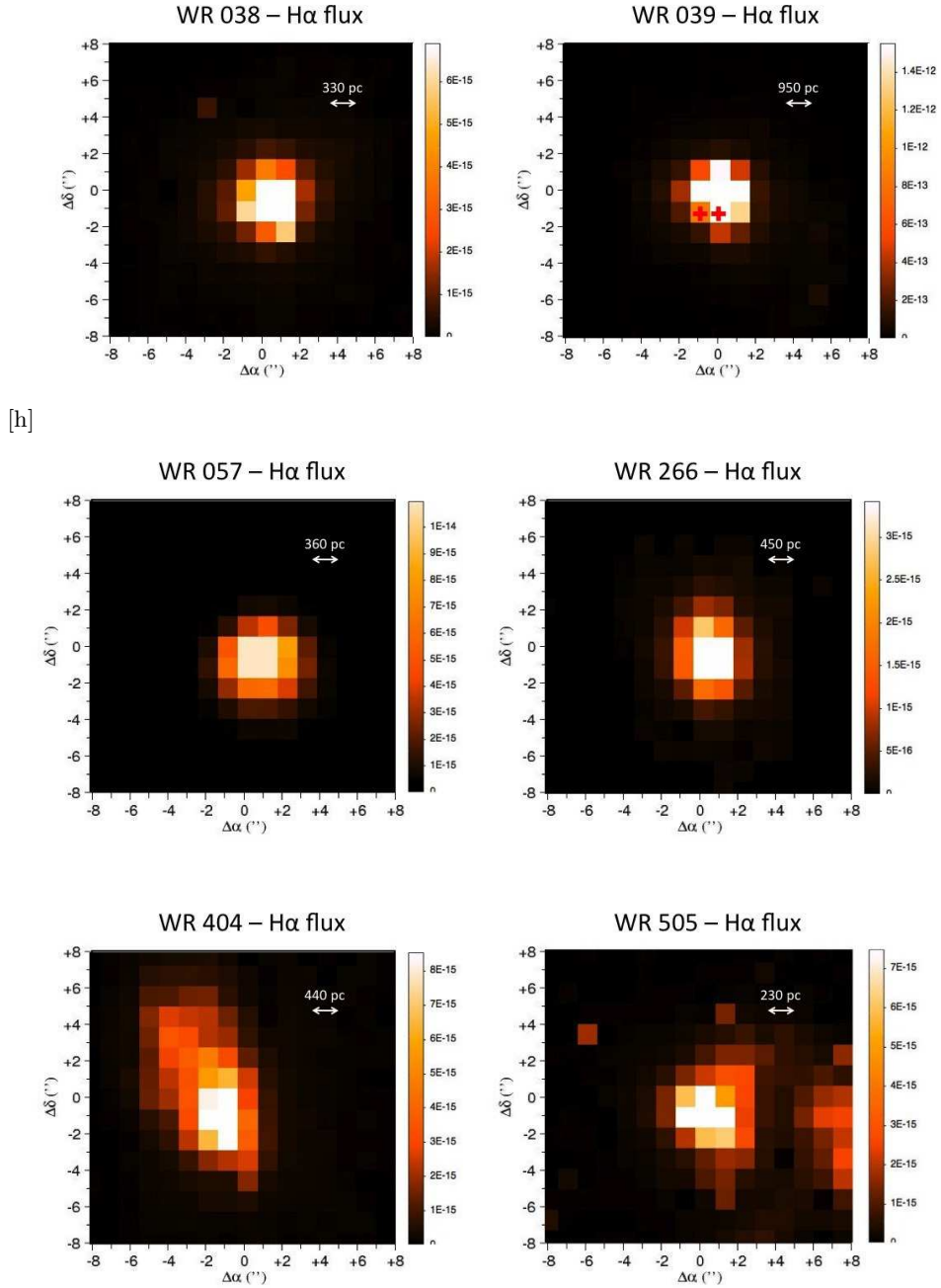


FIGURE 1. Extinction corrected H α maps of the six observed WR galaxies. In all images, each spaxel has 1" of resolution. North is up and east to the left. Fluxes are in units of erg/s/cm². The relative size in parsecs, at the adopted distance of each object, is indicated. For WR038, the spaxels where the WR bump was detected from our PMAS data are marked with red crosses.

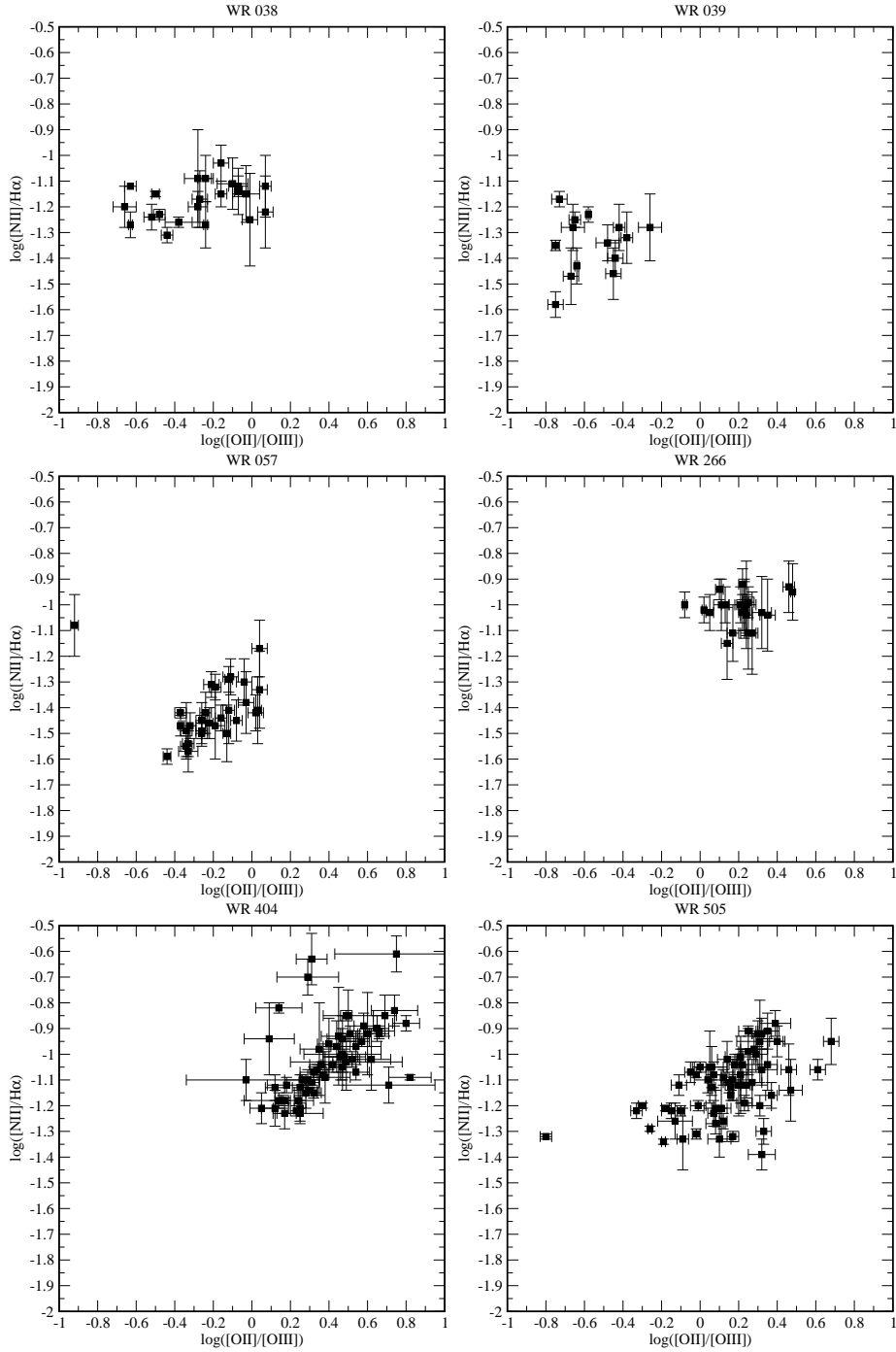


FIGURE 2. Relation between the $[\text{O II}]/[\text{O III}]$ and $[\text{N II}]/\text{H}\alpha$ emission line ratios for those spaxels with sufficient S/N in the four involved lines of the six observed galaxies.

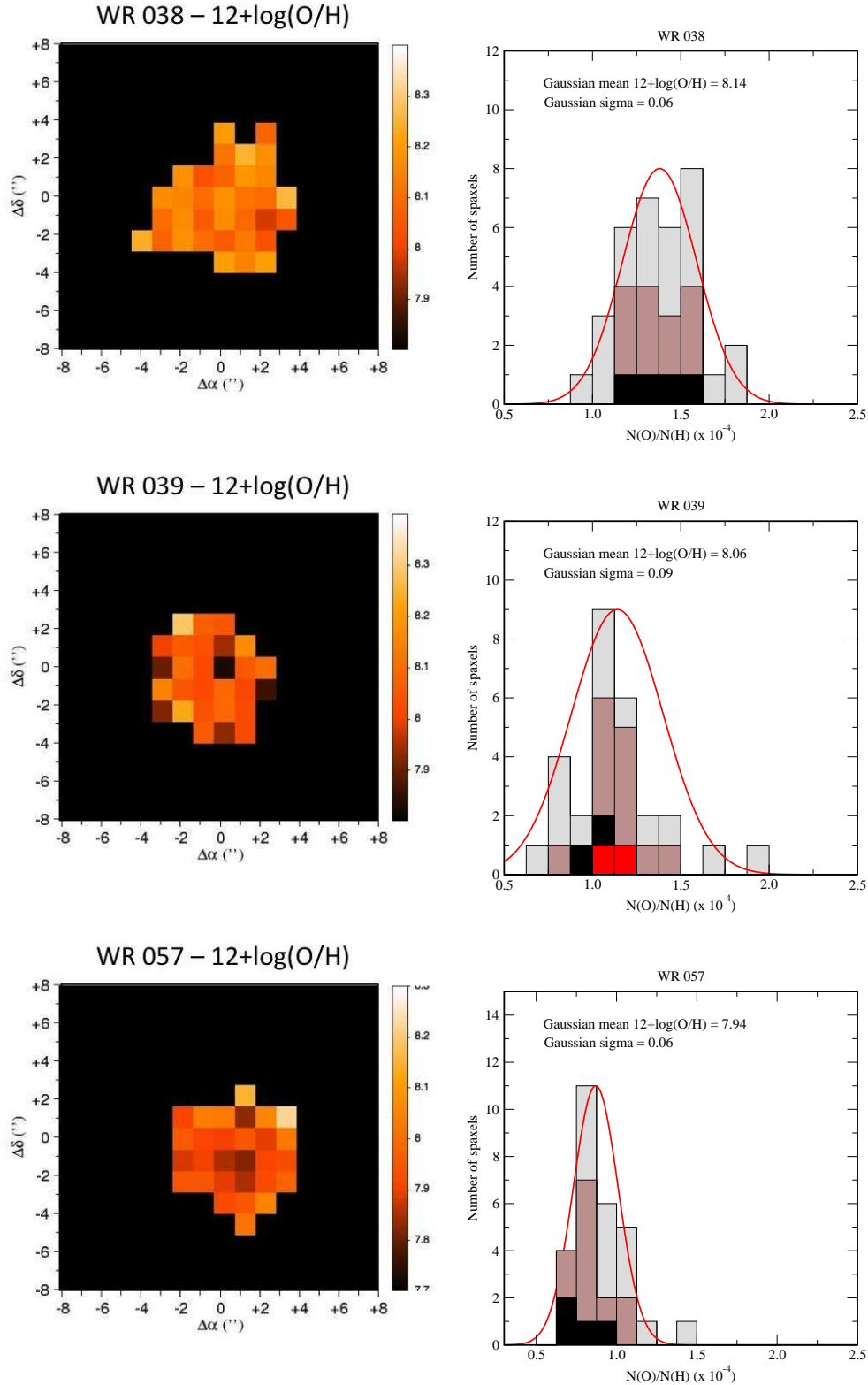


FIGURE 3. Oxygen abundance maps derived as described in the text and histogram distributions in linear scale for WR038, WR039, and WR057. In all images, each spaxel has $1''$ resolution, north is up and east is left. The bars in the histogram represent spaxels with detected WR emission (red), spaxels in the same positions as the SDSS pointing (black), spaxels adjacent to this position (brown), and the other spaxels (grey).

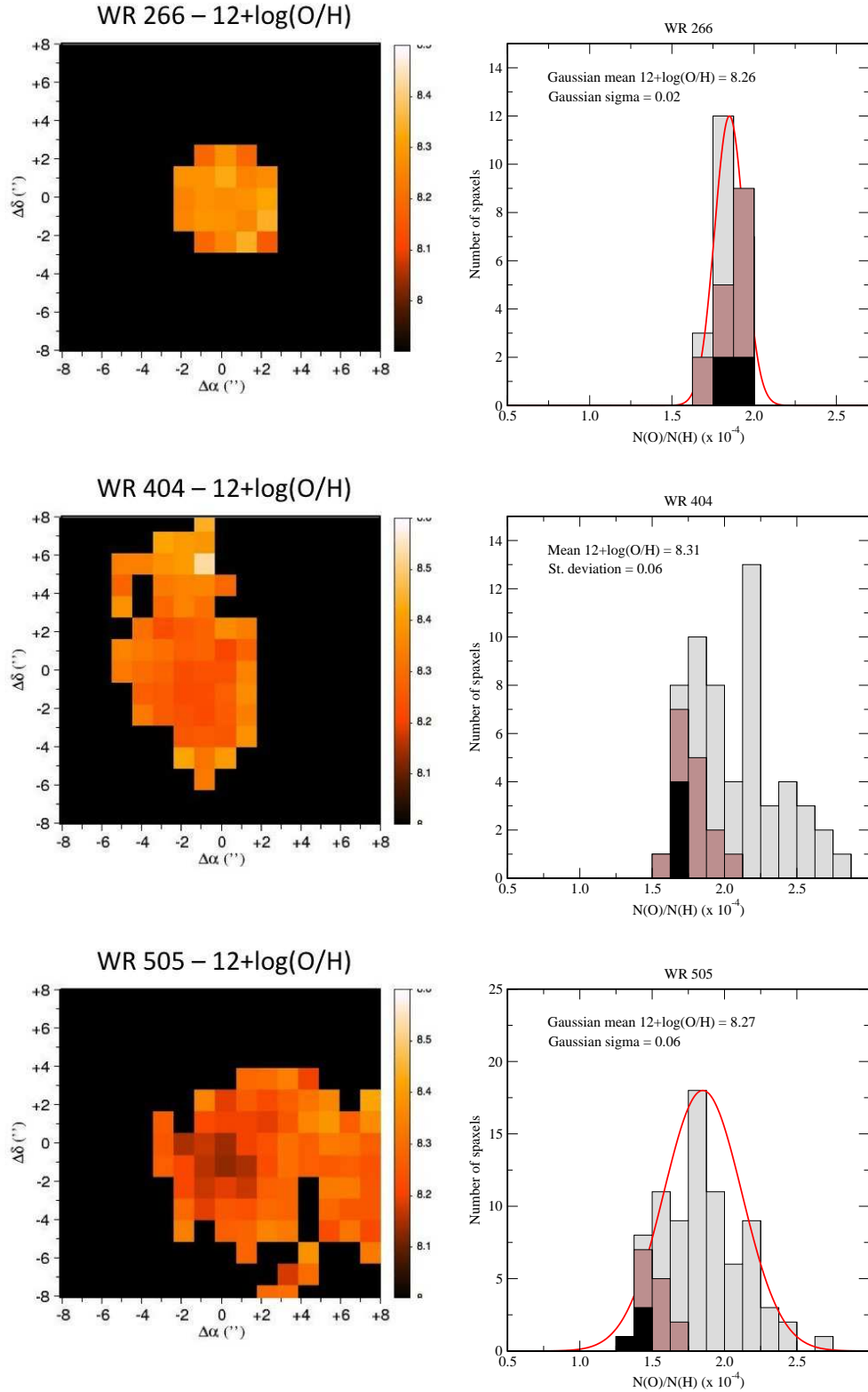


FIGURE 3. (cont.) Same figure for WR266, WR404, and WR505

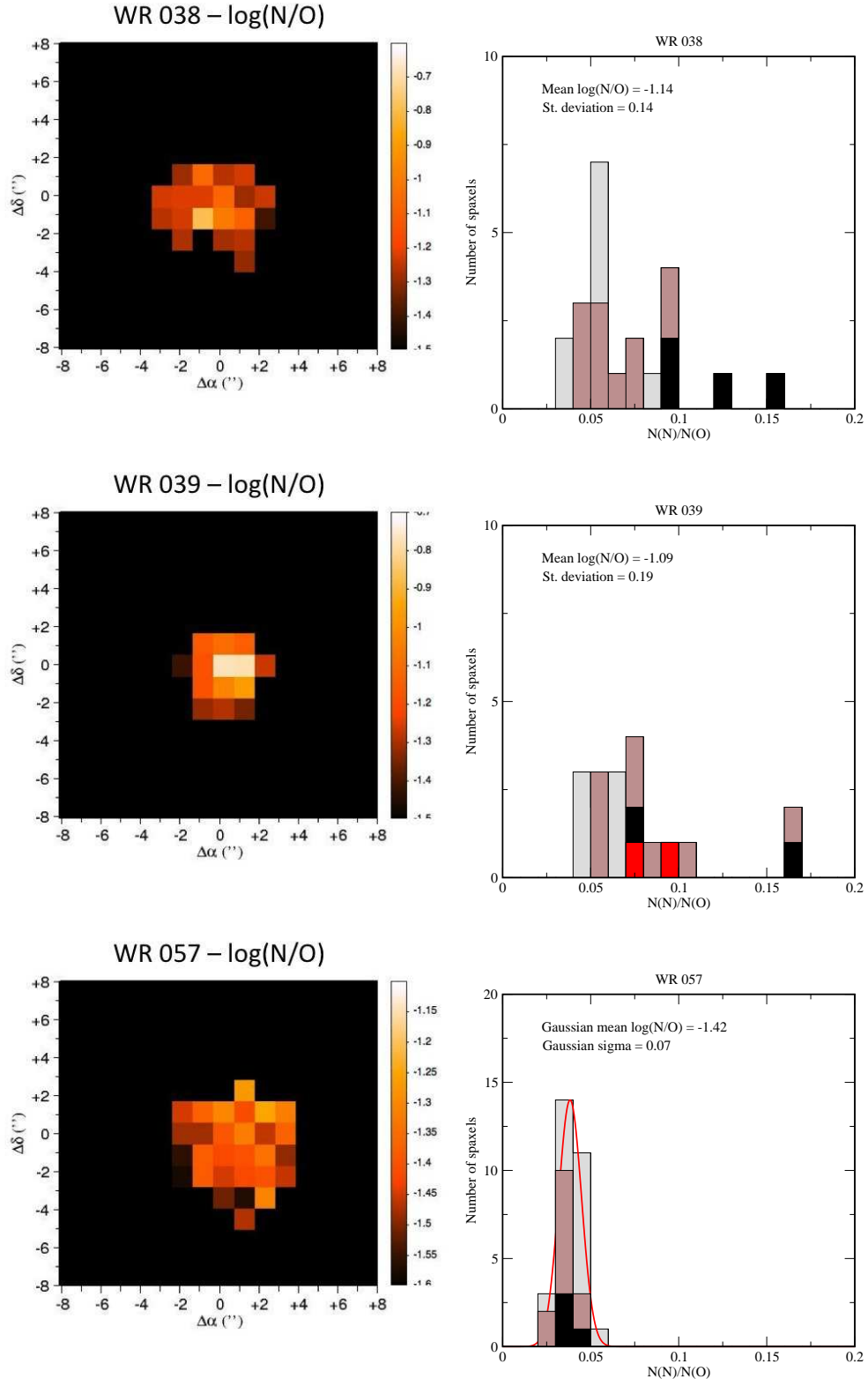


FIGURE 4. N/O ratio maps derived as described in the text and histogram distributions in linear scale for WR038, WR039, and WR057. In all images, each spaxel has 1" resolution, north is up and east is left. The colors in the bars have the same meaning as in Figure 3.

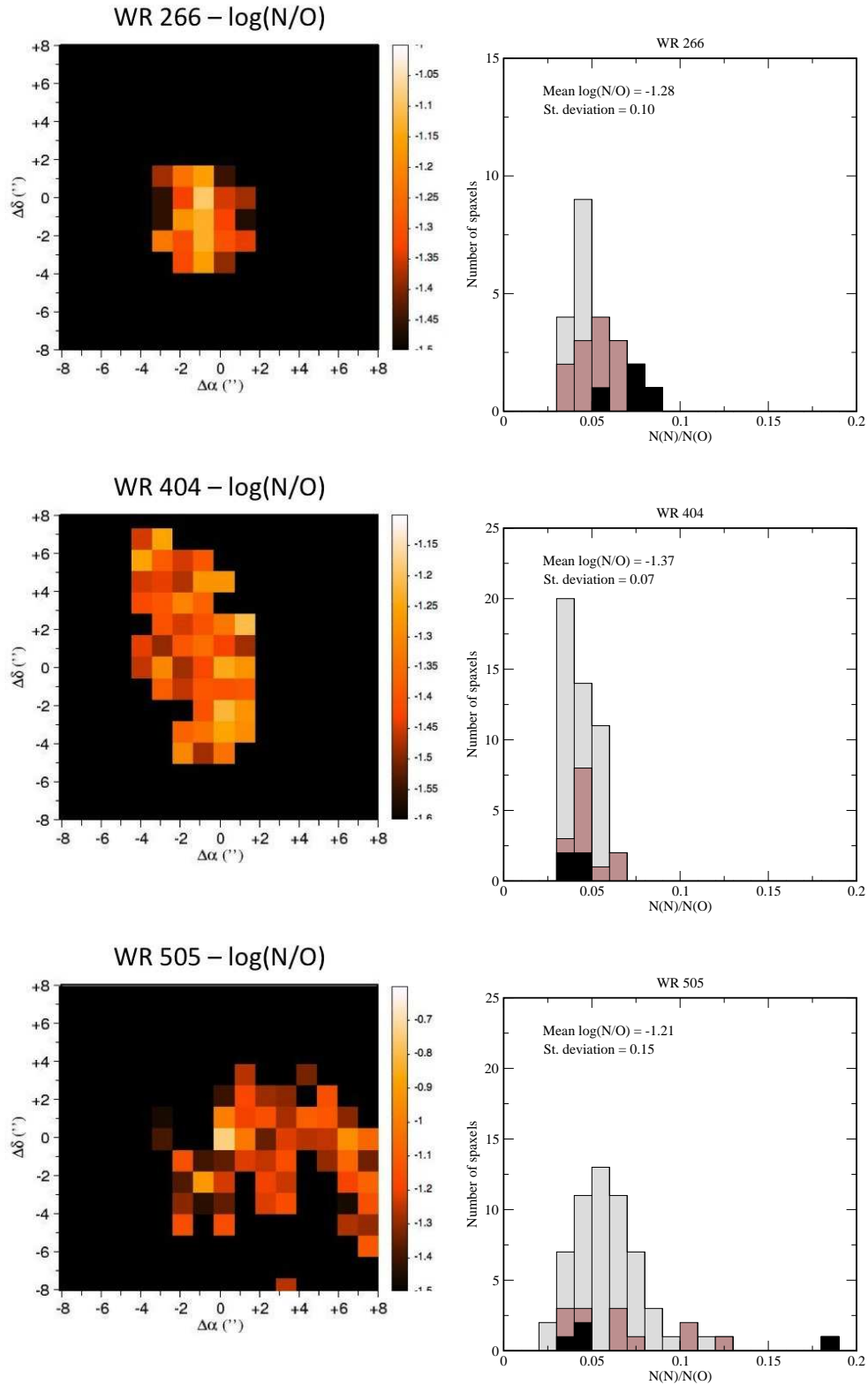


FIGURE 4. (cont.) Same figure for WR266, WR404, and WR505

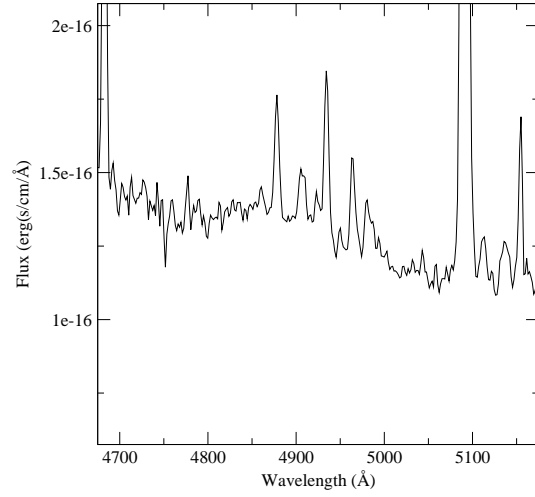


FIGURE 5. Optical spectrum taken with PMAS coadded in the two spaxels in WR038 where the Wolf-Rayet blue bump is detected.

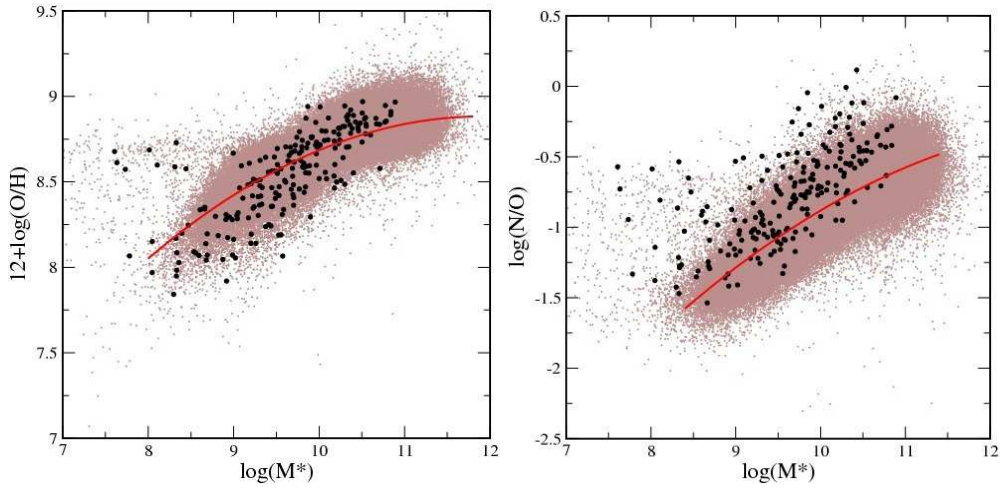


FIGURE 6. MZR (left) and MNOR (right) relations for the star-forming galaxies selected from the SDSS DR7. The solid red lines, calculated by Pérez-Montero et al. (2013), are quadratic fits to the medians in stellar mass bins of 0.2 dex. The black points are the galaxies matching the catalog of WR galaxies by Brinchmann et al. (2008).